



HAL
open science

Portfolio of distribution maps for *Octopus vulgaris* off Mauritania.

Dedah Ahmed-Babou, Hervé Demarcq, Beyah Meissa, Nicolas Bez

► **To cite this version:**

Dedah Ahmed-Babou, Hervé Demarcq, Beyah Meissa, Nicolas Bez. Portfolio of distribution maps for *Octopus vulgaris* off Mauritania.. 2023. hal-03649730v2

HAL Id: hal-03649730

<https://hal.science/hal-03649730v2>

Preprint submitted on 10 Apr 2023

HAL is a multi-disciplinary open access archive for the deposit and dissemination of scientific research documents, whether they are published or not. The documents may come from teaching and research institutions in France or abroad, or from public or private research centers.

L'archive ouverte pluridisciplinaire **HAL**, est destinée au dépôt et à la diffusion de documents scientifiques de niveau recherche, publiés ou non, émanant des établissements d'enseignement et de recherche français ou étrangers, des laboratoires publics ou privés.

Portfolio of distribution maps for *Octopus vulgaris* off Mauritania

Dedah AHMED-BABOU ^{*(1,2,3)}, email : dedah.ahmed-babou@ird.fr, ORCID: 0000-0002-0576-5171

Hervé DEMARCQ(3), email : herve.demarcq@ird.fr, ORCID: 0000-0003-1995-1183.

Beyah MEISSA(1), email : bmouldhabib@gmail.com, ORCID: 0000-0003-4208-636X

Nicolas BEZ(3), email : nicolas.bez@ird.fr, ORCID: 0000-0002-3526-671X

1. IMROP, Nouadhibou, Mauritania.

2. Ministry of Fisheries and Maritime Economy, Nouakchott, Mauritania.

3. MARBEC, IRD, Univ Montpellier, Ifremer, CNRS, INRAE, Sète, France.

Abstract

This study introduces the concept of portfolios of distribution maps, which consist of the reduced set of empirical orthogonal maps that best explain spatial biomass distributions of a given species over time. The approach is demonstrated for the distributions of common octopus (*Octopus vulgaris*) off Mauritania over the last thirty years. The maps in the portfolio are the subset of empirical orthogonal maps that allowed to recover 60% of the spatiotemporal biomass distribution variance and whose temporal weights were significantly correlated with abundance. For octopus during the hot season, one single map explained half of the overall variance of the distribution data, while during the cold season, the portfolio of octopus distribution maps consisted of four maps, with the temporal weights of the second map being negatively correlated with upwelling intensity six months before. The size of each portfolio represents the number of distinct spatial patterns describing octopus spatial distributions. Assuming that specific but hidden processes

* Corresponding author

- 21 explain each biomass spatial distribution of the portfolio, the size of a map portfolio might be interpreted as a proxy
- 22 for system resilience. A small portfolio could reflect systems that are more fragile.
- 23 Keywords: Spatiotemporal distribution data, Maps portfolio, temporal dynamics, Octopus vulgaris.

24 **Introduction**

25 Ecological monitoring and information systems are increasing worldwide. They are key to providing long-term
26 observations, which are particularly important for reference point determination and investigating tipping points and
27 regime shifts. Aside from their maintenance, one of the main challenges associated with these monitoring systems is
28 how to extract scientific knowledge. For example, how to detect spatial patterns that are persistent in time from large
29 sets of georeferenced observations and how to evaluate their temporal stability in conjunction with abundance
30 variability.

31 This study aimed to develop a generic approach for summarizing the overall spatiotemporal information of a long time
32 series of spatial distributions into a portfolio of distribution maps with two elements, one time-dependent and the other,
33 possibly low dimensional, space-dependent. The approach is based on min-max autocorrelation factors (MAF)
34 (Switzer and Green, 1984) that can be seen as an extension of empirical orthogonal functions (EOFs, Lorenz, 1956;
35 Wikle et al., 2019) to deal with the presence of spatial structure in the data. MAF have been widely applied in ecology
36 (e.g. Petitgas et al., 2020; Solow, 1994; Woillez et al., 2009). However, MAF were initially designed to filter out small-
37 scale noise from a set of images. The percentage of variance explained by the selected factors is thus unknown. A
38 recent paper by Bez et al. (2022) suggested that MAF can be appropriately reformulated into Empirical Orthogonal
39 Maps (EOMs) that order the factors according to the percentage of variance explained. The aim of the study by Bez et
40 al. (2022) was to identify the main spatial patterns that shape the dynamics of a stock. The present work defines how
41 the EOMs are formulated and selected to construct a portfolio of maps consisting of a set of maps describing the main
42 spatial patterns governing the biomass distribution of a species. It then investigates the mutual temporal fluctuations
43 of the elements of the portfolio.

44 The ideas developed in this paper are illustrated for common octopus (*Octopus vulgaris*) off Mauritania over the past
45 thirty years. Octopus represents a key species of the Mauritanian marine ecosystem both in ecological terms (Boyle &
46 Boletzky, 1996; Caddy, 1983) and in economic terms. It accounts for more than 70% of cephalopod landings and one
47 third of demersal catches (Khallahi et al., 2020). In 2019, octopus generated 71% of total export value (\$360 million)
48 of fishery products (Société Mauritanienne de Commercialisation Des Poissons “SMCP”, 2020).

49 The current management and conservation of octopus is based on biological and ecological knowledge, in particular
50 its short lifespan of 12 to 14 months (Guerra, 1979; Hernández-López et al., 2001; Mangold and von Boletzky, 1973),

51 its rapid growth (Domain et al., 2000; Mangold, 1983; Sanchez et al., 1998), its high fecundity of 100,000 and 500,000
52 eggs laid by female (O'dor et al., 1978) and its sedentary lifestyle (Hatanaka, 1979; Caverivière et al., 1999). Octopus
53 reproduce only once; males die after mating and females after hatching of offsprings. Therefore, it is essential to ensure
54 a sufficient proportion of the stock has the chance to reproduce to ensure stock renewal. The sedentary nature of the
55 species implies the need for spatialized management to limit the effects local depletion by fishing and thus creates the
56 need for a good knowledge of its spatiotemporal distribution. In Mauritanian waters, two biological rest periods of 1-
57 2 months each have been implemented each year for all demersal fisheries since 2008. These two rest periods reflect
58 the existence of two annual octopus cohorts with distinct spawning seasons (Hatanaka, 1979; Bez et al., 2022). The
59 variability in abundance of this species is mainly a consequence of recruitment fluctuations that are partly dependent
60 on environmental conditions, especially the intensity of upwelling (Caverivière et al., 1999; Otero et al., 2008) and on
61 the two spawning periods taking place under distinct environmental conditions (Faure et al., 2008).

62 Since 1982, a dedicated monitoring system has been developed to support scientific advice to octopus management
63 bodies (Gascuel et al., 2007). It is based on regular scientific surveys with standardized sampling protocols providing
64 information on octopus spatial distributions through time. Using these data, persistent spatial patterns or tipping points
65 of change in spatial distribution can then be tracked. In this study, the portfolio of octopus distribution maps in
66 Mauritanian waters was characterized using data from 63 scientific surveys covering the period 1987- 2019. The size
67 of the portfolio is discussed as a potential proxy for ecosystem resilience.

68 **Materials and methods**

69 **Scientific monitoring surveys**

70 Between 1987 and 2019, the Mauritanian Institute of Oceanographic Research and Fisheries (IMROP) performed 97
71 scientific demersal bottom trawl surveys on the continental shelf. However, only 63 surveys covered the entire
72 continental slope and were therefore kept for analysis in this study (Figure 1a). The sampling protocol was standardized
73 over the entire period and followed a stratified random protocol based on three latitudinal strata (Figure 1). The mean
74 number of hauls was 102 hauls per survey (min = 57, max = 205, but only four exceed 121 hauls), equally distributed
75 in each strata. The survey area was divided into five bathymetric strata (<30m, 30-80m, 80-200m, 200-400m and 400-
76 600m). The sampling covered very coastal areas due to the probable presence of coastal demersal species. The depth
77 covered ranged from 10m to around 600m. The area of the Banc d'Arguin National Park (PNBA) was not covered by

78 the sampling because it is a marine protected area closed to motorized fishing. The observations consisted of the
79 octopus densities expressed in terms of number of individuals per square meter obtained by dividing the catches by
80 the surface of the area swept by the trawl. These were considered as indicator of abundance assuming that gear
81 catchability remained constant. More details on these data are available in Gascuel et al. (2007), Meissa et al. (2013)
82 and Meissa and Gascuel (2015).

83 For each survey, haul positions were randomly selected and mutually independent. The hauls were thus not performed
84 at the same locations each year. However, the method used in this study required that the observations are located at
85 the same positions (regular or not in space) during the entire time series. In order to fulfill this requirement, the data
86 were kriged on a $0.1^\circ \times 0.1^\circ$ grid covering the sampling area before analysis (341 grid cells). Kriging allows estimating
87 the mean octopus density within each grid cell (Chilès and Delfiner, 2000), provided that there were enough hauls in
88 the vicinity. Variogram models were fitted, survey by survey, to the empirical variograms (for the sake of parsimony
89 they are not shown). The input data for the analyses were thus 63 kriging maps and the corresponding abundance
90 indices.

91 A time series of upwelling strength over the same period was built from a monthly dataset of the meridian component
92 (North-South) of composite wind speeds over the Mauritanian zone, 50 to 100 km from the coast. This proxy is
93 considered the best proxy linearly linked to the upwelling index for a North-South oriented coast (Demarcq and Faure,
94 2000), which is the case for the study area.

95 A spatialized time series of seasonal average sea surface temperature (two maps per year, one for the hot season and
96 one for the cold season) on the same spatiotemporal grid as the survey data was built from the National Oceanic and
97 Atmospheric Administration (NOAA) database (NOAA, 2020).

98 Four climatic seasons are generally distinguished in the Mauritanian zone (Dobrovine et al., 1991). A cold season from
99 January to May, a cold-warm transition season from June to July, a hot season from August to October, and a hot-cold
100 transition season from November to December. For this study, these four seasons were aggregated into two main
101 seasons of five and seven months respectively: a hot season from June to October, including 28 of the 63 available
102 surveys and a cold season for the rest of the year (November-May), including the remaining 35 surveys (Figure 1).
103 The precise timing of the surveys within each season was opportunist rather than following a predefined sampling
104 protocol. The temporal spreading of the surveys was however of the same level in each season (similar coefficients of

105 variation; Figure 1). A portfolio of maps was considered for each season. All the calculations were performed in R
106 using the package RGeostats (MINES ParisTech / ARMINES (2022)).

107 **Setting up the portfolio**

108 A portfolio is defined as a selection of relevant empirical orthogonal maps (EOMs). Below the definition of EOMs is
109 recalled and the method to select those included in the portfolio is explained.

110 Building EOMs

111 The workflow for creating empirical orthogonal maps (Bez et al., 2022) is depicted in Figure 2. EOMs are a variation
112 of min-max autocorrelation factors (Switzer & Green, 1984), where the factors are ordered according to their
113 percentage of contribution to the total input variance. The first EOM explains most of the input variance, and so on
114 down to the last EOM that explains little of the input variance.

115 We denote $x_i, i = 1, \dots, S$ the geographical positions of the S grid nodes that were systematically informed (isotopy)
116 at time $t_j, j = 1, \dots, T$, with T being the number of input maps ($S = 341, T = 63$). Input data can be formatted as an
117 $S \times T$ matrix denoted by $Z = Z[i, j] = z(x_i, t_j)$ where each line in Z corresponds to the time series of the value of a
118 given grid cell. Computing EOMs consists of two sequential PCAs. The first PCA, which is nothing but an EOF based
119 on Z , produces an $S \times T$ matrix, denoted Y , with T uncorrelated columns $y(\cdot, t_j)$:

$$120 \sum_{i=1}^S y(x_i, t_j) \cdot y(x_i, t_{j'}) = 0 \quad \forall j \neq j' \quad (1)$$

121 In the spatio-temporal context, each column of Y is a set of georeferenced points, i.e. a map, uncorrelated to each other.
122 The absence of correlation refers to pointwise correlations, therefore, to the absence of correlation between map values
123 for the same geographical point.

124 The second PCA aims at building T new factors $F_j(x_i) = F(x_i, t_j), j = 1, \dots, T$, without mutual spatial correlation for
125 a given spatial distance r (the unit spatial lag corresponds to the grid cell size of the input maps), that is, with the
126 following null scalar products:

$$127 \sum_{i=1}^S [F(x_i, t_j), F(x_i + r, t_{j'})] = 0 \quad \forall j \neq j' \quad (2)$$

128 This second PCA is based on the eigen-decomposition of the matrix of variogram and cross-variogram values between
129 standardized EOFs from the first PCA. Finally, we obtain a set of T new maps called empirical orthogonal maps
130 (EOMs) ordered by decreasing percentage of explained variance. This realizes the decomposition of the initial spatio-
131 temporal variables $z(x_i, t_j)$ into a product of two elements, one element purely spatial made up of the EOMs $F_k(x_i)$
132 and the other element made up of their temporal weights $\psi_k(t_j)$.

$$133 \quad z(x_i, t_j) = m(t_j) + \sum_{k=1}^T \psi_k(t_j) \cdot F_k(x_i) \quad (3)$$

134 where $m(t_j)$ is the average abundance of the input map for time t_j . The weights measure the importance of a given
135 EOM for explaining the survey time series. In other words, the initial set of maps is decomposed into a weighted linear
136 combination of maps without correlation at short scale (blue box in Figure 2). At this stage, the decomposition is
137 performed with no loss of information. EOMs can be computed for raw or standardized maps. The pseudo-algorithm
138 provided in supplementary material highlights the main steps for computing EOMs when the first PCA is applied to
139 standardized maps.

140 The signs of the values of the EOMs and their weights are conventional. Therefore, the interpretation of EOMs and
141 their weights must be established jointly. For example, the interpretation of an EOM whose weights are all negative in
142 the decomposition is strictly equivalent to its symmetry with respect to 0 when taking the symmetry of both the EOM
143 and its weights.

144 By construction, EOMs are mutually uncorrelated for distance 0 and distance r . Assuming that they are also orthogonal
145 for all distances implies that they are fully spatially orthogonal, and that they can be considered as basis for map
146 decomposition. This assumption could be of concern if we were interpolating (i.e. kriging) several EOMs obtained
147 from irregular points in space. In such a case, rigorous interpolation should be done by cokriging the different EOMs.
148 In this study, interpolation was done before the decomposition and we were simply taking linear combinations of the
149 interpolated input maps. Thus, two contrasting situations can be considered: “interpolate first and decompose then” (as
150 in the present case study) where the assumption has no consequence, and “decompose first and interpolate then”, in
151 which case, co-kriging should be recommended to provide a spatially interpolated version of the EOM.

152 Building the portfolio

153 The selection of EOMs for the portfolio is based on two nested steps (dashed orange box in Figure 2). In step one, as
154 it is standard practice in PCA analyses, the number of selected EOM is set to ensure a sufficient part of the variance of
155 the input maps is retained. In the present work, we selected the Q EOMs explaining at least 60% of the input variance.
156 The 60% threshold is arbitrary. It is a compromise between complexity (i.e. the number of EOMs) and explained
157 variance. In our case study, beyond 60% the number of factors increased considerably without a significant gain in
158 explained variance.

159 In step two, among the Q EOMs from step 1 only those are retained whose spatial patterns are connected to the
160 population dynamics of the stock, that is their temporal weights $\psi_k(t_j)$ are correlated with abundance. This is achieved
161 using three complementary criteria. The first criterion is a statistically significant linear correlation between the EOMs'
162 weights and abundance (test level 5%). The second criterion is based on a multivariate time series analysis using auto-
163 and cross-correlograms to identify EOMs whose weights vary smoothly over time (auto-correlogram of weights) and
164 in a consistent manner with regards to the temporal variation of abundance (cross-correlogram between weights and
165 abundances). For this, a linear model of co-regionalization (Chilés and Delfiner, 2000; Goulard and Voltz, 1992)
166 consisting of a nugget effect and a linear part is fitted to the empirical correlograms. This allows modeling and
167 quantifying in a consistent manner the random part and the temporally structured part of the correlations. EOMs to be
168 retained have a small random part (small percentage of nugget effect in the respective auto-correlograms). The third
169 criterion is based on maximizing the covariation in time between abundance and EOM weights. This criterion is
170 evaluated using the slopes of the cross-correlograms between weights and abundance. In linear models of co-
171 regionalization, the (absolute) value of the slope of the cross-correlogram must be smaller than the square root of the
172 product of the slopes of the two auto-correlograms (Chilès and Delfiner, 2009). Thus, the third criterion is that the ratio
173 between the slope of the cross-correlograms and this upper limit is near one. The final selected set of P EOMs ($P \leq Q$)
174 constitute the portfolio of maps summarizing the spatial dynamics of the species for a given season (Figure 2). Note
175 that when a portfolio is made up of several maps, their temporal joint dynamic is accessible through the auto- and the
176 cross-correlograms that were used for the selection of the EOMs entering the portfolio.

177 For each of the two seasons, this methodology is used to build portfolio for octopus and for SST separately.

178 Climatology

179 A climatological spatial distribution pattern can be obtained computing weighted averages of the P maps in the
180 portfolio:

$$181 \quad \bar{z}_P(x_i) = \bar{m} + \frac{\sum_{k=1}^P \bar{\psi}_k \cdot F_k(x_i)}{\sum_{k=1}^P \bar{\psi}_k} \quad (4)$$

182 where $\bar{\psi}_k$ is the mean temporal weight of the P selected EOMs such that:

$$183 \quad \bar{\psi}_k = \frac{1}{T} \sum_{i=1}^T \psi_k(t_j), \quad k = 1, \dots, P \quad (5)$$

184 and where \bar{m} is the mean abundance:

$$185 \quad \bar{m} = \frac{1}{T} \sum_{i=1}^T m(t_j) \quad (6)$$

186

187 **Results**

188 **Portfolio of distribution maps for the hot season**

189 The hot season is the main octopus breeding period (June to October). The first EOM alone restored 47% of the
190 variance of the observed abundance data (Figure 3), and the first three EOMs recover 60% of the initial variance.
191 Amongst them, only the first one was finally selected, the two others ones being not sufficiently correlated with
192 abundance, both statistically and temporally (small coordinate values in Figure 3), and having poorly organized
193 temporal evolutions (small feature size in Figure 3).

194 The hot season's portfolio thus consists only of the first EOM, which is characterized by a north-south gradient, with
195 a high-density area in the north (especially in its wide part), a moderately dense area in the center, and a low density
196 area in the south (Figure 4 , left). The temporal evolution of the weights of the first EOM shows three different phases.
197 There is a sharp decrease over the first five years followed by stability at low level for about 15 years and then a slightly
198 higher level. Most of the signal describing the spatial distribution of octopus abundance is represented by this pattern.
199 This distribution pattern provides information on space occupancy of octopus during this season. It summarizes the
200 historically known pattern of octopus distribution with decreasing abundance from north to south. The years where
201 this pattern had a large weight were years of high octopus abundance during the hot season such as the beginning of
202 the study period. The spatial distribution represented by this EOM is linked to the main breeding season of the species,

203 which takes place at the end of the hot season (September-October). During reproduction, octopus seems to display an
204 affinity to milder water temperatures, which occur to the North of the study area (Figure 5, left).

205 **Portfolio of distribution maps for the cold season**

206 During the cold season the spatio-temporal complexity and thus the size of the portfolio was larger than during the hot
207 season (Figure 3, right). No single EOF spatial pattern was found to be dominant. Indeed, the first EOM explained
208 only 14.7% of the variance of the input distribution data, while the first nine EOMs restored 60% of the variance. Four
209 of these top nine EOMs, respectively the 1st, 3th, 4th and 5th, were linked to the spatiotemporal dynamic of the
210 observed mean gridded survey abundance (density). Their weights depicted significant temporal cross correlation with
211 mean abundance. Together, the four finally selected EOMs to build up the portfolio represented 35.4 % of the initial
212 spatiotemporal variance.

213 The spatial pattern of the first EOM for the cold season was similar to that of the hot season, characterized by an overall
214 north/south gradient with a slightly different temporal evolution (Figure 4, left). However, this EOM showed a denser
215 abundance off the northern area with a more pronounced southward expansion of moderately dense areas. The second
216 EOM of the portfolio (EOM3) indicated a higher abundance in the center with a concentration of abundance south of
217 Nouakchott and two lower density areas in the far south and off the Banc d'Arguin. The EOM4 displayed across-shelf
218 gradient patterns, opposing low density coastal areas to denser offshore areas, particularly in the north and center but
219 also, to a lesser extent, in the south. The last EOM in the portfolio (EOM5) showed two hot spot areas in the north and
220 center. This spatial pattern reinforced, in the north, the spatial pattern of the first EOM but complemented it in the
221 central and southern zones.

222 Given the criteria used for their selection, i.e. correlation with abundance, the EOMs selected for the portfolio had
223 similar long-term temporal variations in their weights (Figure 4, right). The weights decreased at the beginning of the
224 period, then flattened and slightly increased during 2010-2015. This pattern was reflected in the slope of the respective
225 correlograms (Figure 6). However, as indicated by the (quasi systematic) absence of nugget effects in the cross-
226 correlograms, their fluctuations at short temporal scales were not correlated (Figure 6). A noticeable exception
227 concerned the short term negative cross-correlation between EOM1 and EOM3. This reflected the opposite fluctuations
228 of the empirical time series in the middle of the period.

229 The model used in this study quantified the joint temporal dynamics of the EOMs of the portfolio and mean seasonal
230 abundance. It decomposed their mutual temporal correlation into two parts: a nugget effect and a slope. The nugget
231 effect quantified short-term joint fluctuations (e.g. the average variations between two consecutive cold seasons). The
232 slope characterized long-term (multi-annual) joint evolutions. In this context, a change in the overall correlation can
233 be due to either short or long-term processes, or both. However, by construction, the EOMs of the portfolio have been
234 selected because they shared long-term dynamics with that of abundance. By consequence, it remains that within the
235 portfolio the various levels of correlation between EOM weights and abundance rely strongly on the short term. This
236 was consistent with the strong correlation found between EOM' weights and abundance and the value of the nugget
237 effect (Figure 6). In particular during the cold season, the weights of EOM3 were the most strongly correlated to
238 abundance of octopus specifically because, in addition to the fact that they shared similar long-term variations, their
239 short-term fluctuations were also correlated. The cross-correlogram between EOM3 and abundance was indeed
240 proportional to the auto correlogram of abundance (Figure 6). This means that the residual from the regression of the
241 weights of EOM3 against abundance was pure noise, i.e., residuals with no temporal auto-correlation (self-krigeability;
242 Chilès and Delfiner, 2012). In practice, this means that the weights of EOM3 were proportional to abundance over
243 time with some uncorrelated noise (Figure 7). The third EOM represents thus a central spatial pattern of the spatio-
244 temporal dynamic of octopus. It explained around 7 % of the spatial distribution of octopus that is density dependent.

245 The climatological spatial pattern associated with the cold season was characterized by two dense areas rather offshore
246 in the northern zone and coastal in the central zone (**Erreur ! Source du renvoi introuvable.**). A northern zone off
247 Cape Blanc had its epicenter located between the bathymetric lines of 80 and 200m. A second zone was found south
248 of the Cap Timiris (in the middle of the central zone) with an extension to a bathymetric level close to that of the
249 northern zone.

250 The weights of the EOMs that were part of the portfolio were not statistically different (Student p-value = 0.008) for
251 surveys carried out in December and in March (Figure 9). The ranges of fluctuation and the mean densities appeared
252 smaller for December surveys. However, for the two instances where a December survey was followed by a March
253 surveys the following year, the evolutions of the weights were mixed up (increasing for EOM5, decreasing for EOM3,
254 one increasing and the other one decreasing for EOM1 and EOM4).

255 During the cold season, the two months with the largest number of surveys were December and March (Figure 1b).
256 Although not significant, the temporal weights for EOM 1 to 5 were larger in March compared to December (Figure
257 9). March was the month used for analyzing relationships with the upwelling intensity index. Correlations with the
258 upwelling index for the same month (i.e. considering EOM weights during the months of the surveys and the
259 upwelling indices for the same month during the period 1987-2019) and with a time lag of one to seven months
260 before showed similar behavior for each of the EOMs of the portfolio. The correlation is significantly negative only
261 for EOM3 for a 6 months delay (5% level test; Figure 10 left). The upwelling indices in September belonged to the
262 lower part of the interval of fluctuation and corresponded to low upwelling intensity (Balguerías et al., 2002). The
263 eight instances available for this study (octopus survey in March and upwelling index available six months before)
264 covered the full range of possible values observed in September from 1988 to 2019. In particular, they were not
265 distributed in the tails and hence did not represent a particular situation.

266 **Discussion**

267 The approach of portfolios of distribution maps proposed in this paper relies on a set of criteria to select the empirical
268 orthogonal maps to be included in the portfolio. These criteria may be case specific and it is hard to avoid subjective
269 choices. First, similarly to any PCA analysis, one has to choose a threshold for the variance to be explained by the set
270 of selected maps. For a target value of 60% of explained variance, it can happen, as in our case that three and nine
271 maps can be enough for summarizing spatial distributions of octopus in two seasons. The aim of the study being to
272 identify the spatial patterns which were correlated with abundance, we then selected those EOMs whose weights had
273 significant temporal cross-correlations with abundance. This resulted respectively in one and four spatial patterns in
274 each seasonal portfolio explaining 47% and 35 % of the overall variance observed over the past thirty years. In other
275 words, this analysis demonstrated for the first time that half of the information brought by the initial twenty-eight maps
276 recorded between 1987 and 2019 during the hot season could be summarized by a single distribution map whose
277 temporal evolution increased and decreased with octopus abundance. During the cold season, the situation was more
278 complex and the variability could be less easily reduced. Four maps made up the portfolio for that season and their
279 recombination based on their respective weights allowed recovering only a third (35%) of the initial variance. There
280 was thus a more clear and persistent signal for connecting spatial pattern and stock abundance during the hot season,
281 and thus more possibilities for efficient spatial planning during this season.

282 Despitess its importance for explaining the overall variance of the distribution maps observed during the cold season,
283 EOM2 was not selected for the portfolio. Its weights were too variable over time and not sufficiently correlated with
284 abundance, both in the short and in the long term (Figure 3). In other words, EOM2 represented a spatial pattern that
285 was important for explaining the variance of the original set of distributions (hence its rank in the decomposition) but
286 without temporal coherence and without connection to abundance. EOM2 was symptomatic of a coastal hotspot of
287 abundance south of Cap Timiris (Figure 11) that pulses at random from time to time without contributing much to the
288 abundance. The portfolio of the cold season explained not more than a third of the overall variance, which indicates
289 that the spatial distribution of octopus during the cold season were highly variable and poorly linked to abundance
290 variations.

291
292 The derived climatology aimed at representing the average spatial distribution of octopus over the study period
293 accounting for the effects of abundance variations on the spatial distribution. The two seasonal climatologies based on
294 one map for the hot season and on the average of four maps weighted by their average weights for the cold season,
295 showed similar spatial patterns (not shown). This confirms the known yearlong persistence of a gradient of octopus
296 density from north to south (Pease, 1973) whose intensity is related to abundance (stronger in years with higher
297 densities). However, during the cold season, abundance tended to be more offshore with a secondary area of
298 distribution in the middle of the Mauritanian EEZ. The fact that the portfolio was larger during the cold season could
299 be linked to an affinity to optimal water temperatures.

300
301 The spatio-temporal decomposition of the time series of thirty-four SST maps covering the period 1986-2020 for each
302 season provided interesting insights on the spatial distribution of octopus and on the two portfolios generated in the
303 present study. First, during the hot season, 88% of the variance of the SST input maps was represented by a single
304 map. During the cold season, the signal was more blurred. Four maps were needed to recover 67% of the variance (the
305 first one incorporating 38%). This difference in number of maps was similar to the difference between the two
306 portfolios obtained for octopus even though the levels of variance explained by the portfolio (48% and 35%) were
307 notably smaller than the percentage of variance explained by the first x EOMs of SST (? %). Second, the main spatial

308 patterns in both seasons was a north-south gradient. However, the gradient did not mean the same thing in both seasons.
309 According to the literature, an optimal window for octopus would likely be centered on 21°C (Villanueva, 1995). The
310 observed mean SST was around 24°C and 19.5°C during the hot and the cold seasons respectively so that the optimal
311 window is respectively below and above the mean during the two seasons. Values around 21°C corresponded to
312 negative areas in SST EOM1 for the hot season (Figure 5). More precisely, the SST in the northern area of EOM1
313 during the hot season represented an area that was -2°C below the seasonal average. Weighted by 1.5 in the
314 decomposition of the true SST distributions, this area was thus precisely where one finds systematically SST values
315 around 21°C during the hot season. There was thus a very strong match between octopus densities and SST main
316 spatial patterns during the hot season. In the cold season, this gradient was complemented by other patterns accounting
317 for more than 10% each, that were consistent with the patterns observed in the octopus portfolio (more southern, more
318 offshore). Indeed, given the mean SST, the optimal window, if relevant, corresponded to positive areas in the main
319 maps. In particular, the fourth most important pattern presented in the cold season time series corresponded to a clear
320 and strong westwards cross-shelf gradient that can be connected to a similar medium signal found in the octopus
321 portfolio.

322 The fact that the arrangement of maps in terms of the percentage of variance explained (EOM) strongly matched the
323 arrangement based on the strength of their spatial structures (MAF) is worth mentioning (**Erreur ! Source du renvoi**
324 **introuvable.**). The situation could be that the EOMs explaining most of the variance could be maps without spatial
325 structure, i.e. with hot spots appearing here and there from EOM to EOM. This would be the case for systems with
326 strong spatiotemporal fluctuations and poor persistence of their spatial distribution over time. In this study, the maps
327 explaining the most of the variance of octopus spatial patterns are indeed also those with the strongest spatial structures.

328 In an ideal situation, one would work with a regular spread of scientific surveys over time. This was not the case in the
329 present study as the timing of the surveys was somewhat opportunistic. For instance, during the cold season, surveys
330 took place mainly in December (N=10) or in March (N=10) and April (N=8). However, the weights of the EOMs were
331 not associated with specific months and their differences were not statistically significant. Therefore, the four EOMs
332 selected for the portfolio of the cold season (November-May) were considered together as the set of principal spatial
333 patterns that best summarized octopus spatiotemporal distributions during that season. However, the analysis of the
334 joint temporal dynamics of the weights of the different EOMs highlighted the particular characteristics of EOM3.
335 While all EOMs of the portfolio shared their long-term trends with that of abundance, the short-term (i.e. year-to-year)

336 variations of the weights of EOM3 were also correlated with abundance. EOM3 represented thus a major spatial pattern
337 of the spatiotemporal dynamics of octopus. It captured a part of the spatial distribution of octopus that is density
338 dependent. The particular role played by EOM3 was reinforced by the analysis of the correlation with the upwelling
339 intensity index. Amongst the four EOMs making up the portfolio of the cold season, this was the only one whose
340 temporal weights showed significant correlation with the upwelling index when considered six months before. Even
341 though to be interpreted with care given it was based on only eight observations, this result is interesting. While the
342 phenology between upwelling and primary and secondary productions is well documented, the demonstration of a
343 delayed impact on octopus distribution is new. The March surveys caught individuals that weight on average one
344 kilogram (data not shown). These individuals mostly correspond to pre-spawning adults of 9-10 months. They come
345 from the spawning that took place around May the year before. Given the duration of larvae and para-larvae
346 developments (Otero et al., 2007, Domain et al., 2000), the end of the pelagic phase for these individuals falls around
347 August-September. Thus September during which upwelling is usually not intense (Figure 10), coincides with the
348 period of settlement for the individuals spawned in May. Our results suggest that the less intense the upwelling is in
349 September, the more spatially concentrated the octopus recruitment is in the following March, with highest occurrence
350 of octopus off the coast in the central Mauritanian ZEE as indicated by the spatial pattern of EOM3 (**Erreur ! Source**
351 **du renvoi introuvable.**).

352 The present study suggested that a portfolio of distribution maps and in particular its size can provide novel insights.
353 During the hot season, only one EOM was needed to summarize the set of observations for octopus compared to four
354 EOMs for the cold season. The two seasons are of similar durations (five and seven months respectively) and surveys
355 data were spread across both. Thus, the difference in portfolio size between the two seasons is not attributable to
356 variations in the timing of the monitoring. Instead, the difference in map portfolio size could be considered a
357 consequence of a real difference in the spatial dynamics of octopus during the two seasons. The portfolio size quantified
358 the effective number of spatial patterns of octopus seasonal distributions. It was reduced to a single spatial pattern
359 during the hot season in the present study. In contrast, the spatial distribution of octopus during the cold season was a
360 mixture of four principal maps, with the importance (weight) of one being strongly related to the fluctuation of
361 abundance.

362 Ecological considerations arising from portfolio size can be of two kinds. Portfolio size measures the complexity of
363 spatial occupancy patterns and the associated complexity of possible external parameters governing them over time.

364 On the one hand, a large portfolio can characterize systems where one process governing biomass distribution can
365 decrease without impacting the overall system if other processes offset it. On the other hand, systems associated with
366 a small portfolio size have fewer buffer effects and could be more sensitive to external changes (putting all the eggs in
367 one basket is risky). Following these lines, a general perspective of this work could be to quantify the size of many
368 species distribution portfolios and relate them to knowledge about the resilience of the ecosystem the species belong
369 to.

370 **Funding**

371 No funding

372 **Conflict of Interest statement**

373 No conflict of interest.

374 **Author Contributions Statement**

375 DAB and NB conceived the ideas, analysed the data and led the writing of the paper. HD and
376 BM contributed critically to the draft. All authors gave final approval for publication.

377 **Bibliography**

378 Balguerías, E., Hernández-González, C., Perales-Raya, C. 2002. On the identity of *Octopus vulgaris* Cuvier, 1797
379 stocks in the Saharan Bank (Northwest Africa) and their spatio-temporal variations in abundance in relation to
380 some environmental factors. *Bulletin of Marine Science*, 71, 147-163.

381 Bez, N., Renard, D., Ahmed-Babou, D. 2022. Empirical Orthogonal Maps (EOM) and distance between empirical
382 spatial distributions. Application to Mauritanian octopus distribution over the period 1987-2017. *Mathematical*
383 *Geosciences*, 55, 113-128. <https://doi.org/10.1007/s11004-022-10018-w>

384 Boyle, P. R., Boletzky, S. V. 1996. Cephalopod populations : Definition and dynamics. *Philosophical Transactions*
385 *of the Royal Society of London. Series B: Biological Sciences*, 351, 985-1002.
386 <https://doi.org/10.1098/rstb.1996.0089>

- 387 Caddy, J. F. 1983. The cephalopods: Factors relevant to their population dynamics and to the assessment and
388 management of stocks. *Advances in assessment of world cephalopod resources*, 231, 416-449.
- 389 Caverivière, A., Domain, F., Diallo, A. 1999. Observations on the influence of temperature on the length of embryonic
390 development in *Octopus vulgaris* (Senegal). *Aquatic Living Resources*, 12, 151-154.
- 391 Chiles, J. P., Delfiner, P. 2009. *Geostatistics: Modeling Spatial Uncertainty*. John Wiley & Sons.
- 392 Domain, F., Jouffre, D., Caverivière, A. 2000. Growth of *Octopus vulgaris* from tagging in Senegalese waters. *Journal*
393 *of the Marine Biological Association of the United Kingdom*, 80, 699-705.
- 394 Demarcq, H., Faure, V. 2000. Coastal upwelling and associated retention indices derived from satellite SST.
395 Application to *Octopus vulgaris* recruitment. *Oceanologica Acta*, 23, 391-408. [https://doi.org/10.1016/S0399-](https://doi.org/10.1016/S0399-1784(00)01113-0)
396 [1784\(00\)01113-0](https://doi.org/10.1016/S0399-1784(00)01113-0)
- 397 Dobrovine, B., Ould Mohamed Mahfoud, M., Ould Sidina, D. 1991. La ZEE mauritanienne et son environnement
398 géographique géomorphologique et hydroclimatique. *Bulletin Scientifique du CNROP*, 24.
399 <https://aquadocs.org/handle/1834/518>.
- 400 Faure, V., Inejih, C., Demarcq, H., Cury, P. 2008. The importance of retention processes in upwelling areas for
401 recruitment of *Octopus vulgaris*: The example of the Arguin Bank (Mauritania). *Fisheries Oceanography*, 9,
402 343-355. <https://doi.org/10.1046/j.1365-2419.2000.00149.x>
- 403 Gascuel, D., Labrosse, P., Meissa, B., Taleb Sidi, M. O., Guénette, S. 2007. Decline of demersal resources in North-
404 West Africa : An analysis of Mauritanian trawl-survey data over the past 25 years. *African Journal of Marine*
405 *Science*, 29, 331-345.
- 406 Goulard, M., Voltz, M. 1992. Linear coregionalization model: Tools for estimation and choice of cross-variogram
407 matrix. *Mathematical Geology*, 24, 269-286.
- 408 Guerra, A. 1979. Fitting a von Bertalanffy expression to *Octopus vulgaris* growth. *Investigación Pesquera*, 43, 319-
409 326. <https://www.researchgate.net/profile/Angel-Guerra->

410 2/publication/269101025_Fitting_a_von_Bertalanffy_expression_to_Octopus_vulgaris_growth/links/569d2a70
411 08ae16fdf0795eee/Fitting-a-von-Bertalanffy-expression-to-Octopus-vulgaris-growth.pdf

412 Hatanaka, H. 1979. Studies on the fisheries biology of common octopus off the northwest coast of Africa. *Bull. Far*
413 *Seas Fish. Res. Lab.*, 17, 13-124.

414 Hernández-López, J. L., Castro-Hernández, J. J., Hernández-García, V. 2001. Age determined from the daily
415 deposition of concentric rings on common octopus (*Octopus vulgaris*) beaks. *Fishery Bulletin*, 99, 679-684.

416 Khallahi B., Taleb, H. , Barham, C. B., Habibe, B. M, Kane, E. A., Bouzouma, M. E. (Eds). 2020 -Aménagement des
417 ressources halieutiques et gestion de la biodiversité au service du développement durable. Rapport du Neuvième
418 Groupe de Travail de l'IMROP, Nouadhibou, Mauritanie, 11-14 février 2019. 246p. [https://www.imrop.mr/wp-](https://www.imrop.mr/wp-content/uploads/2020/10/Rapport-scientifique-GT2019.pdf)
419 [content/uploads/2020/10/Rapport-scientifique-GT2019.pdf](https://www.imrop.mr/wp-content/uploads/2020/10/Rapport-scientifique-GT2019.pdf) : not peer reviewed.

420 Lorenz, E. N. 1956. Empirical orthogonal functions and statistical weather prediction. Massachusetts Institute of
421 Technology, *Department of Meteorology Cambridge. Statistical forecasting project, Scientific report 1.*

422 Mangold, K. 1983. Octopus vulgaris. In Boyle, P. R. (ed.), *Cephalopod Life Cycles (I): Species Accounts*. Academic
423 Press, Orlando: 335-363.

424 Mangold, K., von Boletzky, S. 1973. New data on reproductive biology and growth of *Octopus vulgaris*. *Marine*
425 *Biology*, 19, 7–12. <https://doi.org/10.1007/BF00355414>

426 Meissa, B., Gascuel, D., Rivot, E. 2013. Assessing stocks in data-poor African fisheries: A case study on the white
427 grouper *Epinephelus aeneus* of Mauritania. *African Journal of Marine Science*, 35, 253-267.

428 Meissa, B., Gascuel, D. 2015. Overfishing of marine resources: Some lessons from the assessment of demersal stocks
429 off Mauritania. *ICES Journal of Marine Science*, 72, 414-427.

430 National Oceanic and Atmospheric Administration 2020, Global Coral Bleaching Monitoring, 5km, V.3.1,
431 Monthly,1985-Present.
432 [https://coastwatch.pfeg.noaa.gov/erddap/griddap/NOAA_DHW_monthly.html?sea_surface_temperature%5B\(
433 2021-06-15T23:00:00Z\)%5D%5B\(89.975\):\(-89.975\)%5D%5B\(-](https://coastwatch.pfeg.noaa.gov/erddap/griddap/NOAA_DHW_monthly.html?sea_surface_temperature%5B(2021-06-15T23:00:00Z)%5D%5B(89.975):(-89.975)%5D%5B(-)

434 179.975):(179.975)%5D&.draw=surface&.vars=longitude%7Clatitude%7Csea_surface_temperature&.colorBa
435 r=%7C%7C%7C%7C%7C&.bgColor=0xffccccff

436 Pease, N. 1973. Fisheries of Mauritania, 1971. <https://repository.library.noaa.gov/view/noaa/30110>

437 O'dor, R. K., Wells, M. J. 1978. Reproduction versus somatic growth: hormonal control in *Octopus vulgaris*. *Journal*
438 *of experimental Biology*, 77, 15-31.

439 Otero, J., González, Á. F., Sieiro, M. P., Guerra, Á. 2007. Reproductive cycle and energy allocation of *Octopus vulgaris*
440 in Galician waters, NE Atlantic. *Fisheries Research*, 85, 122-129.

441 Otero, J., Álvarez-Salgado, X. A., González, Á. F., Miranda, A., Groom, S. B., Cabanas, J. M., Casas, G., Wheatley,
442 B., Guerra, Á. 2008). Bottom-up control of common octopus *Octopus vulgaris* in the Galician upwelling system,
443 northeast Atlantic Ocean. *Marine Ecology Progress Series*, 362, 181-192.

444 Petitgas, P., Renard, D., Desassis, N., Huret, M., Romagnan, J.-B., Doray, M., Woillez, M., Rivoirard, J. 2020.
445 Analysing Temporal Variability in Spatial Distributions Using Min–Max Autocorrelation Factors: Sardine Eggs
446 in the Bay of Biscay. *Mathematical Geosciences*, 52, 337-354. <https://doi.org/10.1007/s11004-019-09845-1>

447 MINES ParisTech / ARMINES (2022). *RGeostats: The Geostatistical R Package*. Version: [12.0.1] Free download
448 from: <http://cg.ensmp.fr/rgeostats>.

449 Sanchez, F. J., Iglesias, J., Moxica, C., Otero, J. J. 1998. Growth of octopus (*octopus vulgaris*) males and females
450 under culture conditions. *International Council for the Exploration of the Sea (ICES)*, CM 1998/M:47.

451 Solow, A. R. 1994. Detecting change in the composition of a multispecies community. *Biometrics*, 50, 556-565.

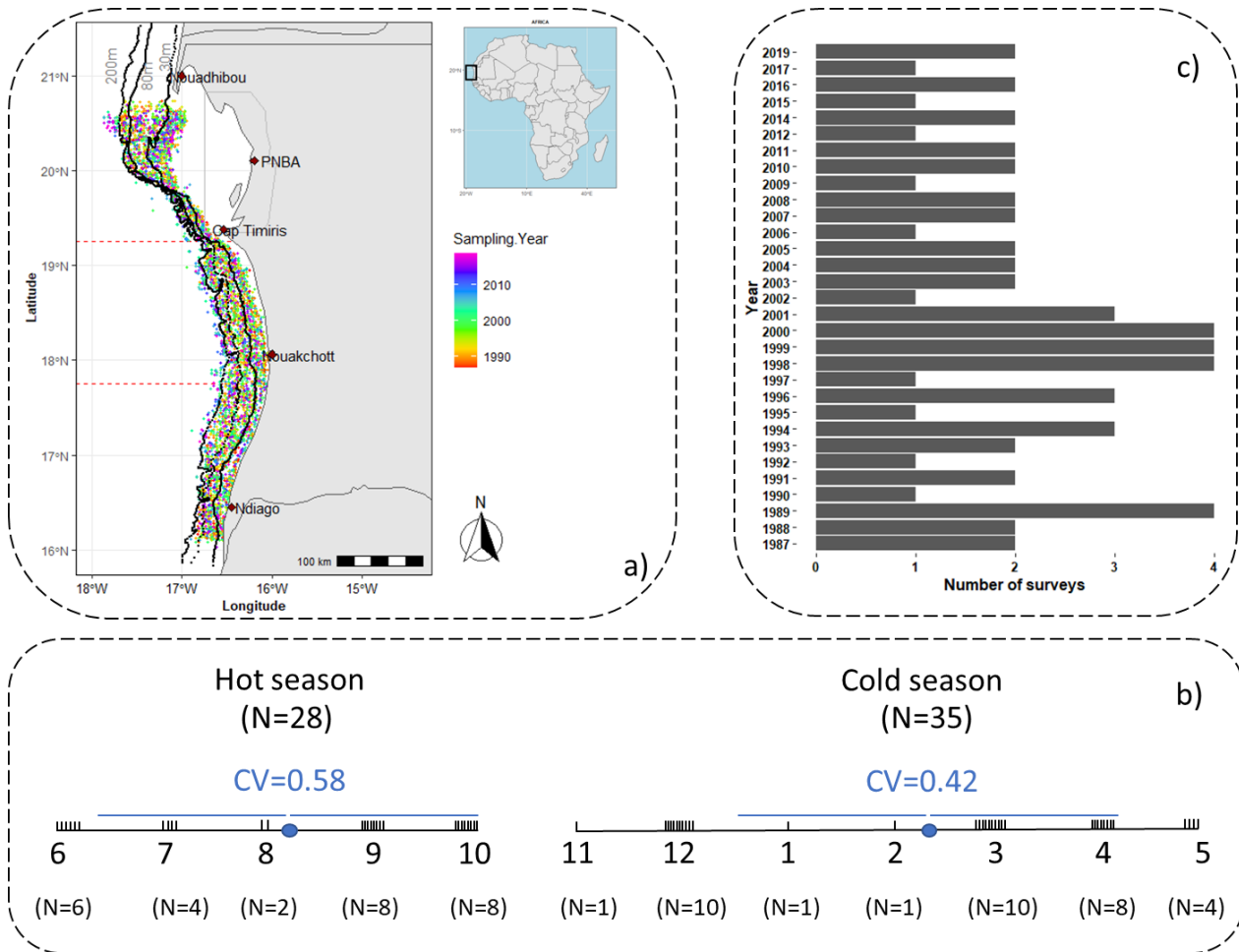
452 Société Mauritanienne de Commercialisation Des Poissons. SMCP–SEM, 2020. Bulletin de statistiques 2019 Version
453 42. <http://dtf.gov.mr/images/2019/SMCP2019.pdf>: not peer reviewed.

454 Switzer, P., & Green, A. A. 1984. Min/max autocorrelation factors for multivariate spatial imagery. Technical report
455 6, *Department of Statistics, Stanford University, CA*.

456 Villanueva, R. 1995. Experimental rearing and growth of planktonic *Octopus vulgaris* from hatching to settlement.
 457 *Canadian Journal of Fisheries and Aquatic Sciences*, 52, 2639-2650.

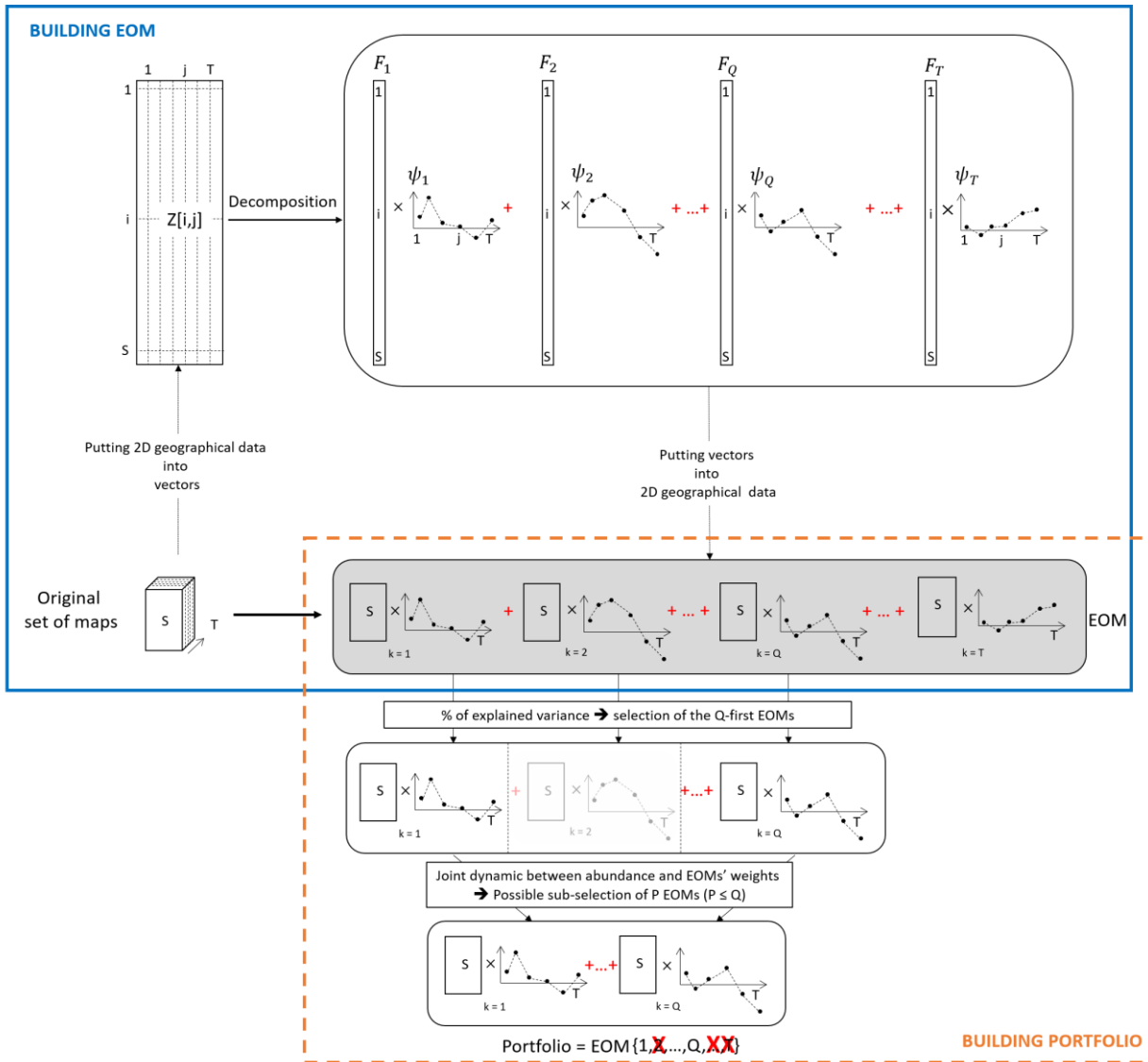
458 Wikle, C. K., Zammit-Mangion, A., Cressie, N. A. C. 2019. Spatio-temporal statistics with R. Chapman and Hall/CRC.

459 Woillez, M., Rivoirard, J., Petitgas, P. 2009. Using min/max autocorrelation factors of survey-based indicators to
 460 follow the evolution of fish stocks in time. *Aquatic Living Resources*, 22, 193-200.



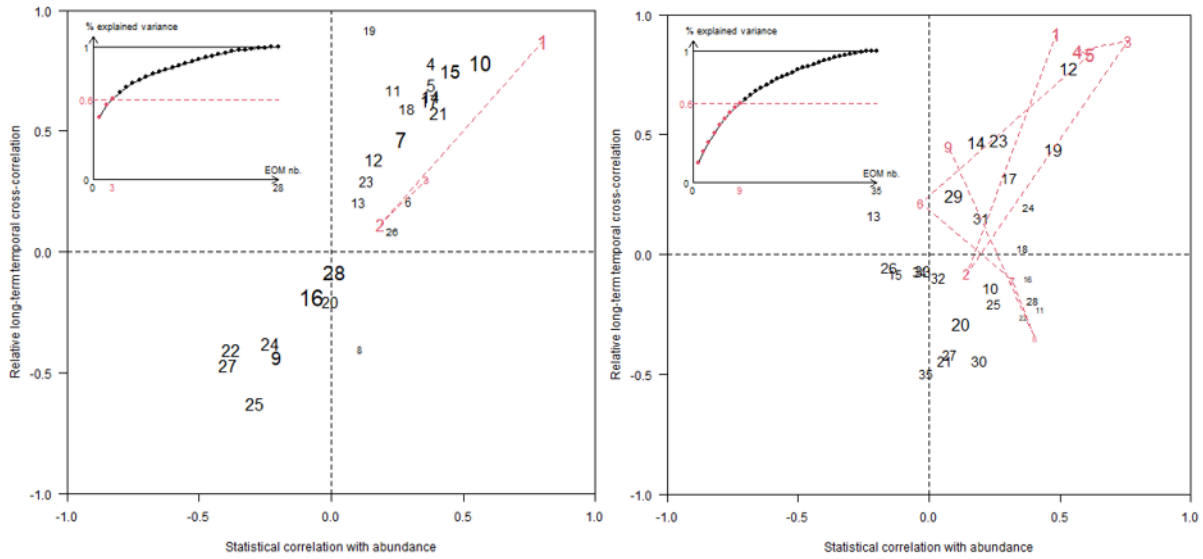
461

462 *Figure 1 (a) Spatial distribution of sampling stations during the study period. PNBA = Parc National du Banc*
 463 *d'Arguin. The three latitudinal strata (North, 20°36'N-19°15'N; Central, 19°15'N-17°45'N; and South, 17°45'N-16°03'N)*
 464 *are represented by dashed lines. (b) Timing of the surveys (month) for each of the hot and cold seasons. The mean and*
 465 *coefficient of variation of the timing of the surveys by season are given in blue. (c) Number of surveys per year.*



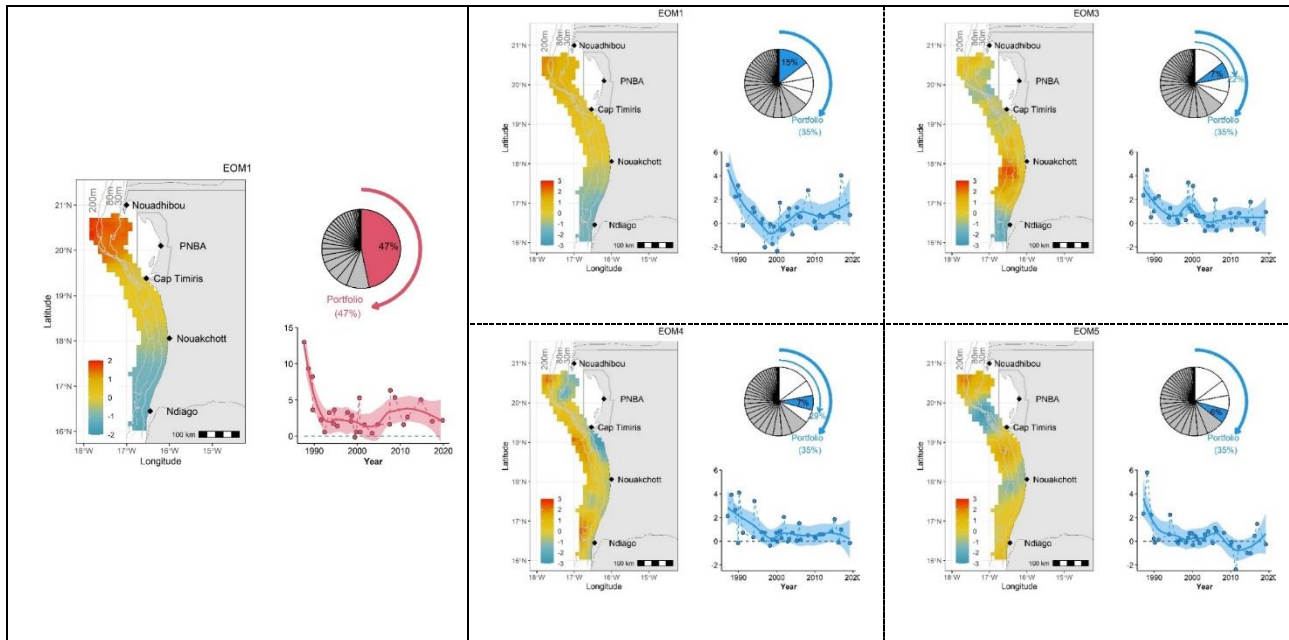
467

468 *Figure 2 Workflow of the method. Upper blue block: building T different EOMs from a set of T maps. Lower orange*
 469 *block: selecting the P EOM entering the portfolio. In this case, the Q-first EOMs explain a given percent of the overall*
 470 *variance. Amongst them, the second EOM is not retained as its weights are not sufficiently correlated to the temporal*
 471 *fluctuations of abundance.*



472

473 *Figure 3 Criterion used to define the distribution map portfolio for octopus in Mauritanian waters for the hot (left)*
 474 *and the cold (right) season. The inset panels represent the percentage of variance explained when including*
 475 *progressively more and more EOMs. The threshold of 60% was used for selecting the candidate EOMs for building*
 476 *the portfolio. The main graph shows the position of EOMS with respect to their relationship with octopus abundance.*
 477 *The x-axis corresponds to the correlation between EOM weights and abundance (the closer to +/- 1, the better). The*
 478 *y-axis represents the relative values of the slopes of the cross-correlograms between each EOM weights and*
 479 *abundance, with respect to the maximum possible value (the closer to +/- 1, the better). The size of EOF numbers is*
 480 *inversely proportional to the percentages of nugget effect in the auto-correlograms of the EOMs' weights (the larger*
 481 *the better). The EOMs that allow recovering 60% of the input variance are indicated in red and connected for better*
 482 *visibility.*



484 *Figure 4 Portfolio of octopus during the hot (left - red) and the cold (right - blue) seasons over the entire study period.*

485 *Each plot is made of an EOM with the temporal evolution of its weights, smoothed by a loess method with a span*

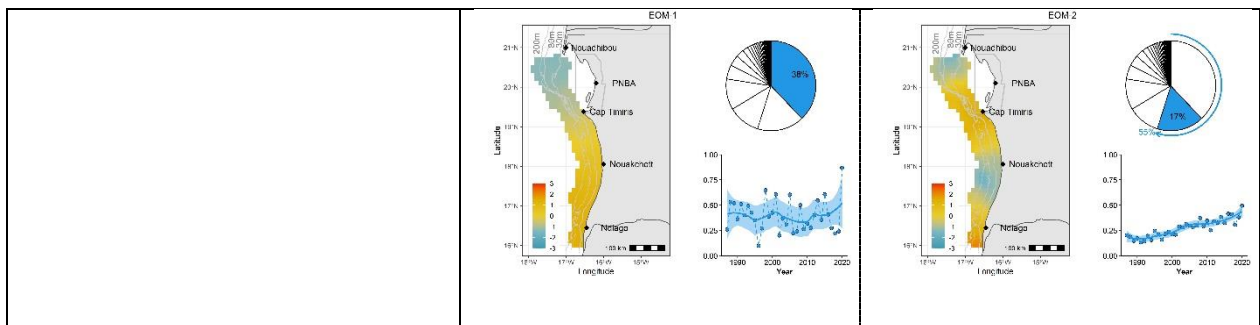
486 *parameter value of 0.5 and associated 95%-confidence interval. Pie chart indicate the percentage of variance*

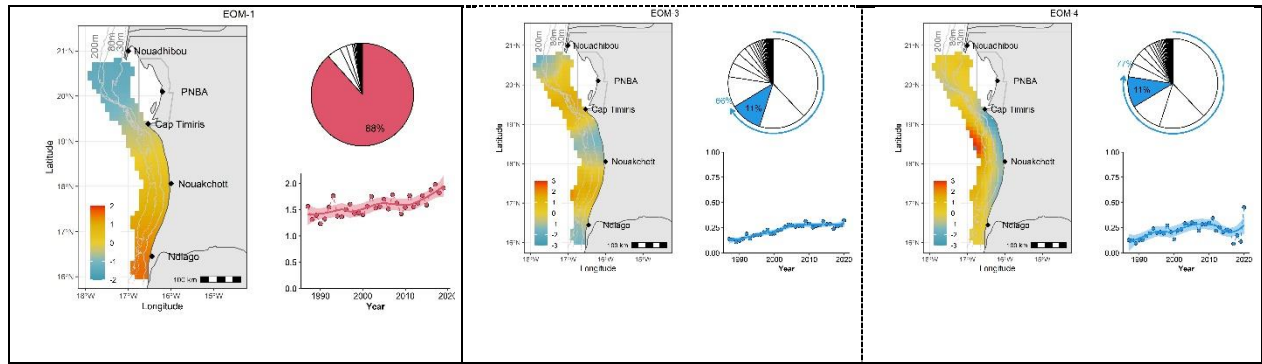
487 *explained by the EOM (arrows represent the cumulative percentage of variance explained by the current EOM and*

488 *the previous ones and the percentage of variance explained by the portfolio). The EOMs that were not selected for the*

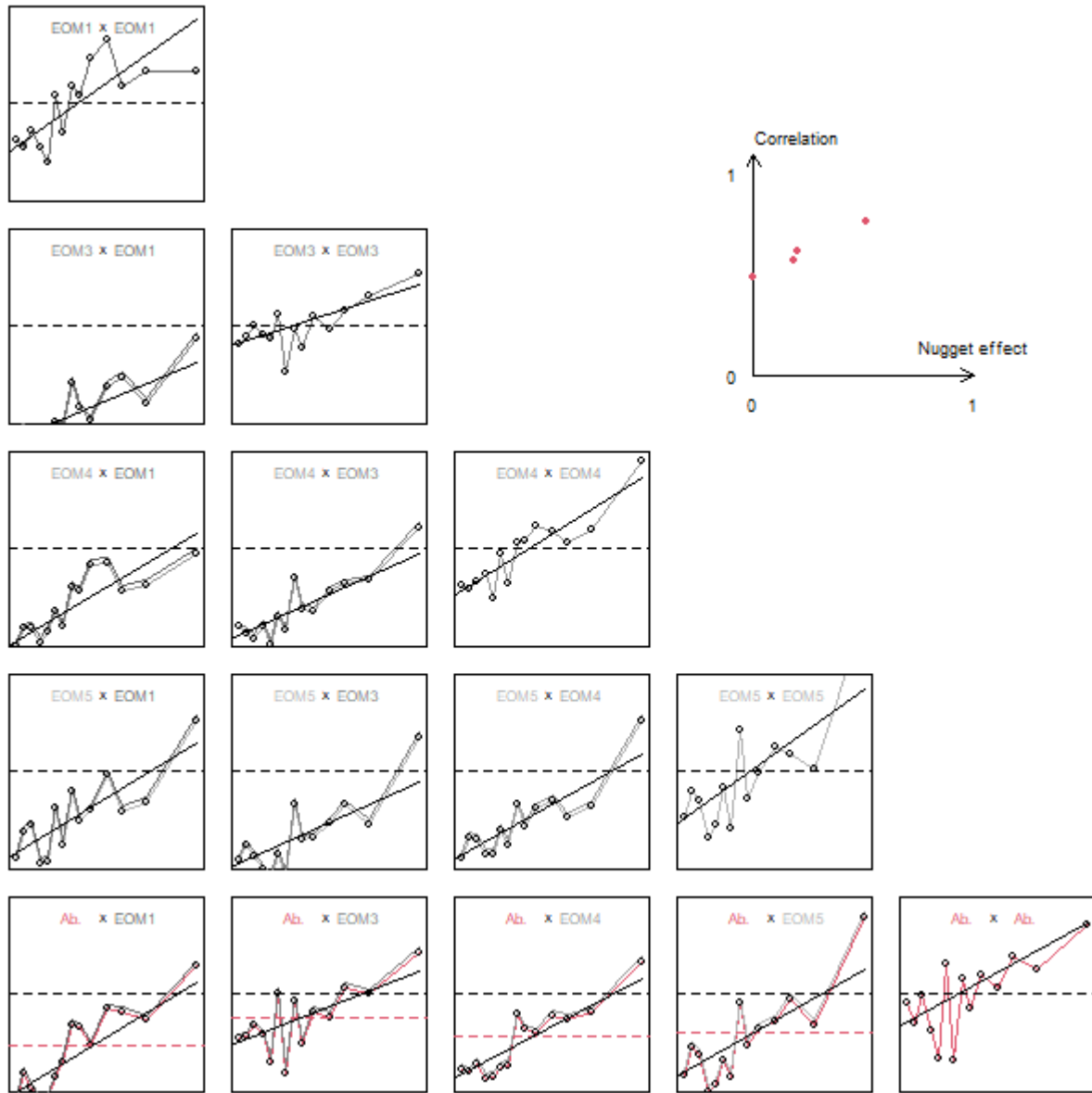
489 *portfolio are represented in grey.*

490





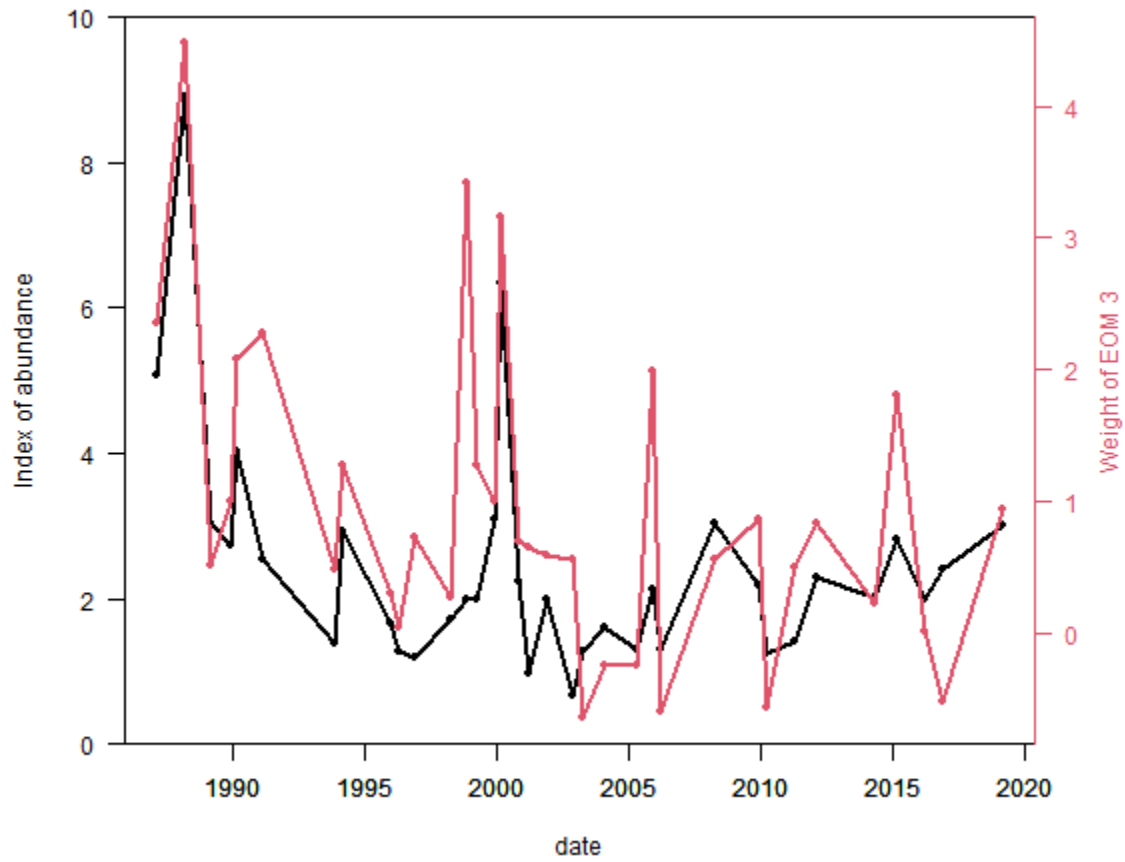
491 *Figure 5. Portfolio of SST during the hot (left - red) and the cold (right - blue) seasons over the entire study period.*
 492 *Each plot is made of an EOM with its weights (smoothed by nonparametric loess with a span parameter value of 0.5*
 493 *and associated 95%-confidence interval) and a pie indicating the percentage of variance explained by the EOM*
 494 *(arrows represent the cumulative percentage of variance explained by the current EOM and the previous ones).*
 495



497

498 *Figure 6 Analysis of the temporal dynamics of the principal spatial patterns (EOM 1, 3, 4, 5) and of the abundance*
 499 *for the cold season. Diagonal panels: auto-correlograms; Lower triangle panels: cross-correlograms. For all panels,*
 500 *the x-axis represents time lags in years (from 0 to 30 years) and the y-axis represents correlations. The horizontal*
 501 *black dashed line is at 1. For off diagonal panels, the horizontal dotted lines represent the correlations. The panels of*
 502 *the last line concerns the cross-correlograms of EOM weights with abundance and the auto correlogram for*
 503 *abundance (last panel). The horizontal red dashed lines represents the correlation between EOM weights and*
 504 *abundance. The linear model of coregionalisation is represented as a continuous line (nugget effect + slope). The*

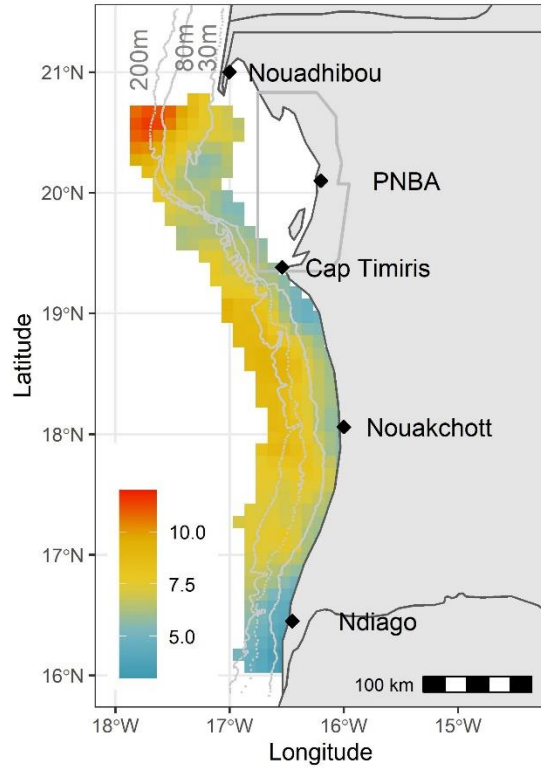
505 *isolated panel represents the correlation between abundance and EOM weights as a function of the nugget effect in*
506 *the model.*



507

508 *Figure 7 Cold season. Time series of the abundance (black) and temporal weights of EOM3 (red).*

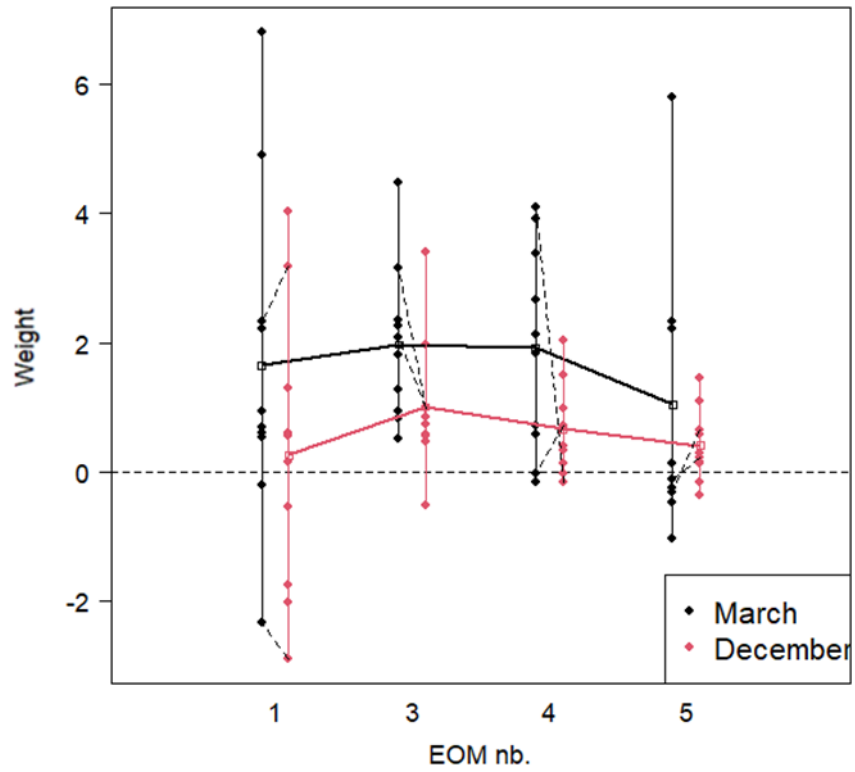
509



510

511 *Figure 8. Climatology for the cold season. This corresponds to the mean of the EOMs selected in the portfolio*
 512 *weighted by their mean weights. The scale is consistent with the input octopus densities (i.e. nb of individual per m²).*

513



514

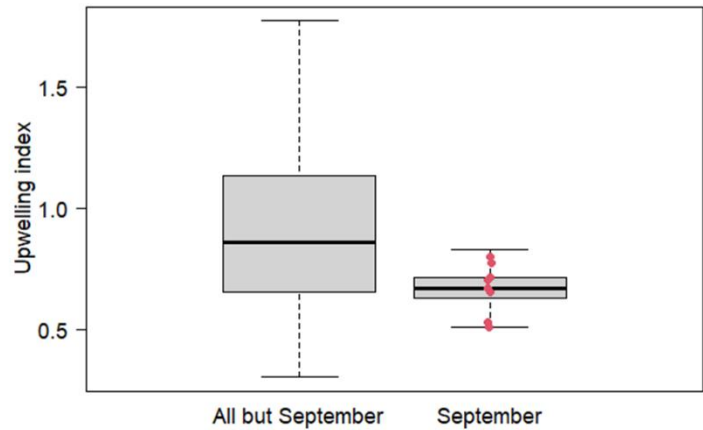
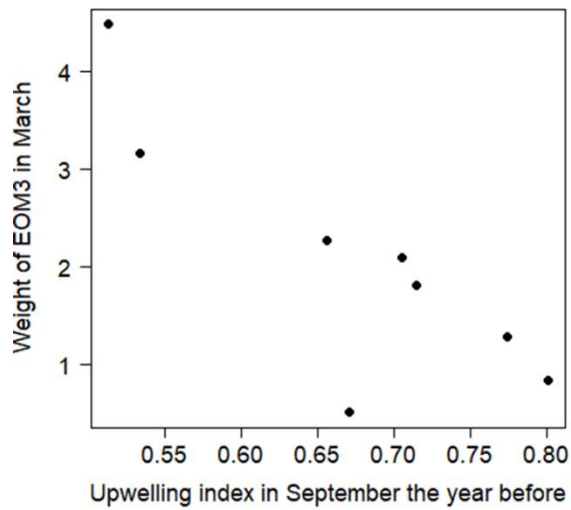
515 *Figure 9 Portfolio for the cold season. Distribution of the EOMs' weights as a function of the EOM numbers for March*

516 *and December surveys. The weights for the surveys carried out in March (N=10) are represented in black. The weights*

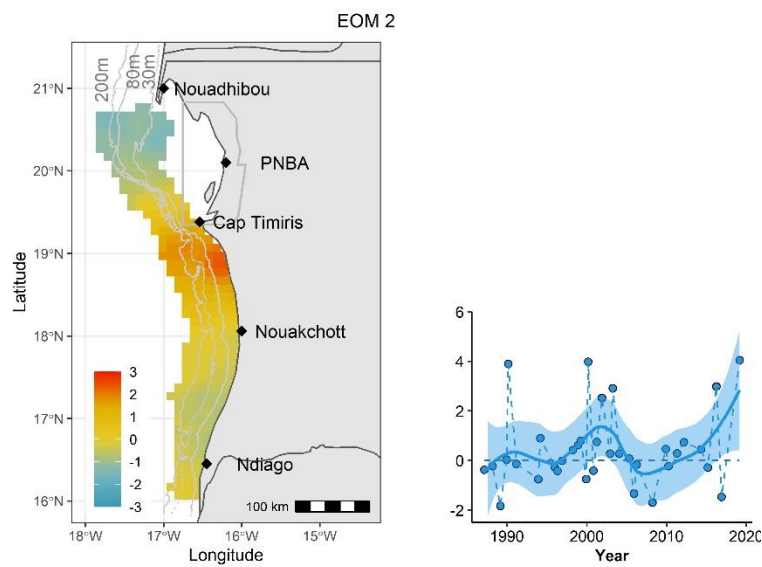
517 *for surveys performed in December (N=10) are given in red. The average values are superimposed. For the two*

518 *instances where a December survey is followed by a March surveys three months later, the evolutions of the weights*

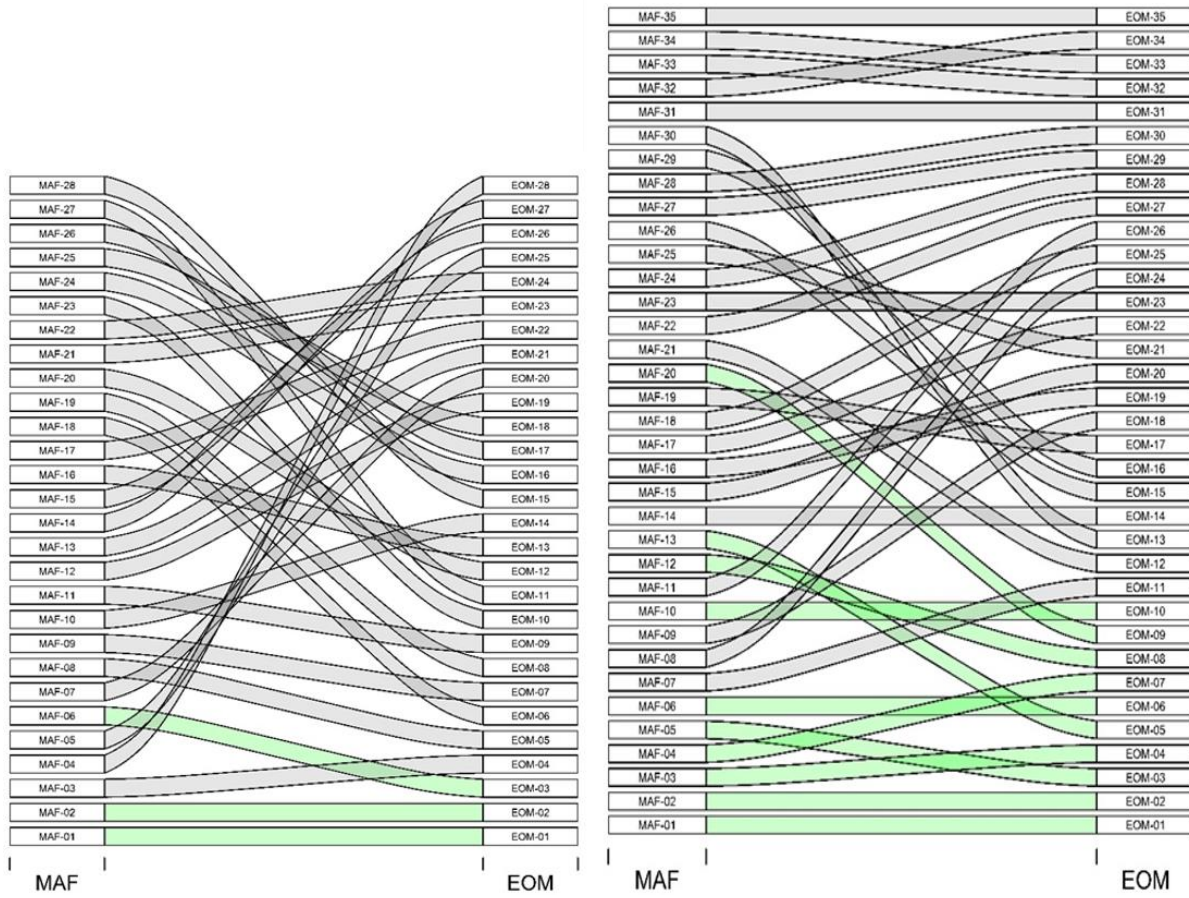
519 *are represented by dotted segments.*



520
 521 *Figure 10 Portfolio of the cold season. Correlation between the weights of EOM3 and the upwelling index. Left: lagged*
 522 *correlations between EOM3 weights in March and the upwelling index 6 months earlier. Right: boxplot of upwelling*
 523 *indices for all months except September versus upwelling indices in September (i.e. 6 months before March). In red*
 524 *the values for the nine years when a survey was performed in March with concomitant upwelling observations.*



525
 526 *Figure 11. Left: Empirical Orthogonal Map EOM2 of octopus for the cold season. This EOM was not selected for the*
 527 *portfolio. Right: temporal evolution of its weights smoothed by a loess method with a span parameter value of 0.5 and*
 528 *associated 95%-confidence interval.*



529

530 *Figure 12 Comparison between the MAF and the EOM arrangements for the hot (left) and the cold (right) season for*
 531 *octopus in Mauritanian waters. The green connections concern the Q first EOMs explaining 60% of total variance.*

532